Theor Chem Acc (2011) 130:1001–1008
DOI 10.1007/s00214-011-0987-8

REGULAR ARTICLE

Structural and thermodynamic properties of Au_{2-20} clusters

Yi Dong · Michael Springborg · Ingolf Warnke

Received: 24 April 2011 / Accepted: 28 June 2011 / Published online: 12 July 2011

Abstract Isolated neutral gold clusters with 2–20 atoms are studied theoretically using a parametrized density-functional tight-binding method combined with genetic algorithms. The structural and energetic properties are analyzed by studying the total energy per atom, the relative stability, the overall shape, and through a common-neighbor analysis. In addition, the temperature dependence of the vibrational heat capacities of the optimized gold clusters has been studied for the first time. We find the vibrational heat capacity of the clusters to be strongly size dependent at low temperature. For instance, the cluster with 6 atoms has a high vibrational heat capacity at low temperature, a finding rationalized in terms of structure.

Keywords Gold clusters · Structural properties · Vibrational heat capacity

Dedicated to Professor Akira Imamura on the occasion of his 77th birthday and published as part of the Imamura Festschrift Issue.

Electronic supplementary material The online version of this article (doi:10.1007/s00214-011-0987-8) contains supplementary material, which is available to authorized users.

Y. Dong · M. Springborg (✉)
Physical and Theoretical Chemistry, University of Saarland, Campus B2.2, 66123 Saarbrücken, Germany
e-mail: m.springborg@mx.uni-saarland.de

Y. Dong
e-mail: y.dong@mx.uni-saarland.de

I. Warnke
Department of Chemistry, University of California, Irvine, CA 92697, USA
e-mail: ingolf.warnke@uci.edu

1 Introduction

From a theoretical point of view, one of the largest challenges in the study of metal clusters is related to the determination of their ground-state structures. In experimental studies, the clusters are rarely isolated, nor in a gas phase or in a rare-gas matrix, but they interact with a medium like a solvent or a supporting surface. Moreover, they may possess surfactants and, in many cases, their precise size is only approximately known. On the other hand, theoretical studies most often deal with isolated well-defined cluster sizes and consider naked clusters without ligands.

Without any further information, identification of the ground-state structure of an N atomic cluster requires a search in a $3N - 6$ dimensional structure space. This computationally very demanding step limits theoretical studies to small clusters.

To overcome the high computational demand, theoretical studies of cluster properties have to incorporate one or more approximations: (1) selected sizes and/or structures of the clusters are studied, (2) empirical potentials that depend only on the interatomic distances are employed, whereby electronic degrees of freedom are neglected, and/or (3) parametrized methods that include electronic degrees of freedom are used. In addition to the use of approximate methods for the determination of the total energy for a given structure, various approaches for the determination of the structure of the global total-energy minimum have been used. These include Simulated Annealing, Basin–Hopping and Genetic Algorithms [1–9].

Gold clusters constitute a special case and have attracted much attention during the past 30 years. However, it has turned out to be particularly difficult to determine the properties of gold clusters, partly because the calculated structures very sensitively depend on the applied methods

[10]. This is to a much lesser extent the case for most other elemental clusters.

Interesting results are obtained by studying the clusters' thermodynamic properties experimentally or theoretically. The melting temperatures of small clusters [11–13] (i.e., temperatures at which the heat capacity as a function of temperature has a maximum) as well as other low-temperature properties can provide useful information.

In this contribution, we shall present results of a theoretical study of the properties of gold clusters. We have used an approximate density-functional methods for the description of the interatomic interactions together with genetic algorithms for the determination of the structure of the global total-energy minimum. Due to the approximations inherent to the applied density-functional method, our results for specific systems may suffer from minor inaccuracies. We stress, however, that our goal is to identify general trends in the size development of the properties of the gold clusters and not in obtaining very accurate results for selected sizes and/or structures. Those could be obtained with the use of more accurate theoretical approaches that, on the other hand, for computational reasons would not permit a more general study like the one presented here.

In the present work, we shall at first (Sect. 3.1) review our earlier results on the structural and energetic properties of gold clusters [14]. As an extension of that work, we shall subsequently (Sect. 3.2) present new results devoted to the vibrational contributions to the thermodynamic low-temperature properties of the clusters. The purpose of the last part is to explore which kind of information can be obtained by studying the heat capacities of the clusters and, in particular, to see whether the heat capacities can be correlated to structural and/or energetic properties of the clusters. We shall, thereby, use the simplest possible approach for studying the heat capacities, i.e., a harmonic approximation for the structures at $T = 0$ and, in addition, also consider temperatures well above those for which anharmonic effects or melting are important. Moreover, we shall not take into account the possibility that there may be more energetically low-lying isomers that all may contribute to the properties of the system for $T \neq 0$, but only consider the single structure of the lowest total energy. However, for the purpose of identifying correlations between heat capacities on the one side and structural and stability properties on the other side, our approach should be justified. Finally, due to the surprising structural properties of gold clusters, these provide an excellent playground for such studies.

2 Computational method

We have used a parametrized density-functional tight-binding (DFTB) method [15] in combination with genetic algorithms to study neutral gold clusters with sizes ranging from 2 to 20 atoms. The DFTB method is used for calculating the total energy of a given structure and for relaxing this structure to its nearest local total-energy-minimum structure. The genetic algorithms are employed for finding the global total-energy-minimum structures. The DFTB method provides some information about the clusters' electronic properties.

The DFTB method is based on the density-functional theory of Hohenberg and Kohn [16] in the formulation of Kohn and Sham [17]. The total energy of the compound of interest relative to that of the isolated atoms is then written as a difference in the orbital energies of the compound, $\{\epsilon_i\}$, minus those of the isolated atoms, augmented by pair potentials,

$$E = \sum_i \epsilon_i - \sum_m \sum_i \epsilon_{im} + \sum_{m_1,m_2} U_{m_1 m_2}(|\mathbf{R}_{m_1} - \mathbf{R}_{m_2}|). \quad (1)$$

Here, ϵ_i is the energy of the ith orbital of the compound, whereas ϵ_{im} is the energy of the ith orbital of the mth isolated atom.

In order to calculate the orbital energies, the Kohn–Sham orbitals Ψ_i of the system of interest are expanded in terms of atom-centered localized basis functions, $\{\phi_{jm}\}$,

$$\Psi_i(\mathbf{r}) = \sum_{jm} c_{ijm}\phi_{jm}(\mathbf{r} - \mathbf{R}_m), \quad (2)$$

where ϕ_{jm} is the jth basis function centered at atom m, placed at point $\mathbf{R}_m$.

The Kohn–Sham single-particle operator is written as

$$\hat{h} = \hat{t} + V_{\text{eff}}(\mathbf{r}), \quad (3)$$

where $\hat{t}$ denotes the kinetic-energy operator and V_{eff} $(\mathbf{r})$ denotes the effective Kohn–Sham potential. The latter is approximated as a simple superposition of the potentials of the neutral atoms

$$V_{\text{eff}}(\mathbf{r}) = \sum_m V_m^0(|\mathbf{r} - \mathbf{R}_m|). \quad (4)$$

We assume that $\langle\phi_{j_1 m_1}|V_m^0|\phi_{j_2 m_2}\rangle$ vanishes unless at least one of the two basis functions is centered at $\mathbf{R}_m$. Thereby, all relevant information for the secular equation can be extracted from accurate density-functional calculations on the two-atomic molecules.

After having determined all quantities for the first two terms in Eq. 1, the short-ranged pair potentials $U_{m_1 m_2}$ as functions of interatomic distance are determined by requiring that the total energy of two-atomic systems (in our case, of Au_2) as a function of interatomic distance, which is determined through accurate density-functional calculations, is accurately reproduced.

Finally, in the present study, we use the same parameter values as in our earlier study on Au_N clusters [14]. This

means that only the 5*d* and 6*s* electrons of the isolated Au atom are explicitly included in the calculations, whereas the rest is treated within a frozen-core approximation. For the Au_N clusters with even N, we considered only singlet states and for odd N only doublet states. Spin-orbit couplings are not directly included in the calculations, although their effects are partly included indirectly through the short-ranged pair potentials.

For the gold structure optimizations, we have used a genetic algorithm which we developed in earlier studies on HAlO clusters [18]. Genetic algorithms are based on the principles of natural evolution and are, therefore, also called evolutionary algorithms [19]. They have been found to provide an efficient tool for global geometry optimizations.

Our version of the genetic algorithms functions as follows. Suppose that we have optimized the structure of the cluster with N atoms. From this structure, we construct a set of initial structures (i.e., the first generation) consisting of M independent clusters for the $(N + 1)$-atom system by randomly adding one Au atom and letting these structures relax to their nearest total-energy minima. Subsequently, M new $(N + 1)$-atomic clusters (i.e., the next generation) are constructed by cutting each of the original ones randomly into two parts that are interchanged (under the constraint that no atom should be too close to any other atom or too far away from all the other ones) and, subsequently, relaxing the resulting structures to their nearest total-energy minima. Out of the total set of $2M$ structures, the M energetically lowest ones are chosen to constitute the next generation. This procedure is repeated many times until the lowest total energy remains unchanged for a large number of generations. The lowest total energy structure is then taken for the global minimum. Global optimization procedures such as the present genetic algorithm cannot explore the entire $(3N - 6)$ dimensional potential energy hypersurface, so that one can never be absolutely certain to have found the global total-energy minimum, i.e., the most stable gold-isomer. Experience has, however, shown that genetic algorithms are among the most reliable unbiased methods for the determination of the structure of the global total-energy minimum.

In addition to the globally optimized structures, we also considered other geometries. Among those were various planar structures for $N \leq 14$ taken from [20–22]. Moreover, we also considered a planar structure for $N = 15$ by adding a single atom to the planar geometry for $N = 14$, making it maximally symmetric. To complete the study, we also considered an icosahedral structure for $N = 13$ and a tetragonal structure for $N = 20$ from [23].

As an extension to our earlier study, we have calculated vibrational properties of the clusters. We apply the Normal Mode Harmonic Oscillator (NMHO) approximation [24] and assume, accordingly, that the structural dependence of the total energy E, when expanded in a Taylor series, can be terminated after the 2nd order terms. Then, the vibrational frequencies, ω_i, are the square roots of the eigenvalues of the dynamical matrix with the elements

$$D_{ij} = \frac{1}{\sqrt{M_i M_j}} \quad f_{ij} = \frac{1}{\sqrt{M_i M_j}} \frac{\partial^2 E}{\partial q_i \partial q_j}. \tag{5}$$

Here, i and j represent two of the $3N$ cartesian coordinates, denoted q_i and q_j, of the cluster atoms, and M_i and M_j are the corresponding nuclear masses.

We use a finite-difference approximation to calculate the force constants f_{ij},

$$\begin{aligned} f_{ij} &= \frac{\partial}{\partial q_i}\frac{\partial E}{\partial q_j} = \frac{\partial}{\partial q_j}\frac{\partial E}{\partial q_i} = \frac{1}{2}\left(\frac{\partial}{\partial q_i}\frac{\partial E}{\partial q_j} + \frac{\partial}{\partial q_j}\frac{\partial E}{\partial q_i}\right) = \frac{-1}{2}\left(\frac{\partial F_i}{\partial q_j} + \frac{\partial F_j}{\partial q_i}\right) \\ &\simeq \begin{cases} \frac{-1}{4\Delta s}\left[F_i(q_j + \Delta s) - F_i(q_j - \Delta s) + F_j(q_i + \Delta s) - F_j(q_j - \Delta s)\right] & i \neq j \\ \frac{-1}{2\Delta s}\left[F_i(q_i + \Delta s) - F_i(q_i - \Delta s)\right] & i = j. \end{cases} \end{aligned} \tag{6}$$

Δs is a small finite coordinate change, and $F_m(q_n \pm \Delta s)$ denotes the mth component of the force on the structure which results from a shift $\pm\Delta s$ of coordinate n. We found that for Δs around 0.001 a.u., the results are essentially insensitive to variations in Δs. Therefore, we have chosen $\Delta s = 0.001$ a.u. in the present calculations.

Finally, from the calculated vibrational frequencies and with the use of Boltzmann statistics, we can calculate the vibrational heat capacities

$$C_{\text{vib}} = k_B \sum_{i=1}^{\text{NVM}} \frac{\alpha_i^2 e^{\alpha_i}}{(e^{\alpha_i} - 1)^2} \tag{7}$$

with

$$\alpha_i = \frac{\hbar\omega_i}{k_B T} \equiv \frac{T_i}{T} \tag{8}$$

and k_B being the Boltzmann constant. NVM is the number of non-zero frequencies and equals $3N - 6$ ($3N - 5$) for non-linear (linear) systems. Moreover, we associate each vibrational mode i with a characteristic temperature T_i. T_i is related to the temperature ($T \simeq 2.35\ T_i$) at which the contribution of the given mode changes most rapidly as a function of temperature. At $T \simeq 2.35\ T_i$, the contribution of the ith mode equals roughly 64% of its maximal contribution (at $T \to \infty$).

Finally, it is easily seen that

$$\begin{aligned} \lim_{T\to\infty} C_{\text{vib}} &= \text{NVM} \times k_B \\ &= \text{NVM} \times 8.6 \times 10^{-5}\,\text{eV/K} \\ &\sim \text{NVM} \times 8.3\,\text{J/(K mol)}. \end{aligned} \tag{9}$$

Thus, from the equipartition theorem, we get that the 6 or 5 rotational and translational modes give a contribution of 25 or 21 J/(K mol) to the heat capacity per cluster. This value is reached for the temperatures we shall consider.

3 Results and discussion

3.1 Structural and energetic properties

We applied the method outlined above for studying properties of neutral gold clusters with sizes $N = 2$–20 atoms. The resulting structures are shown in Fig. 1. In Fig. 2, we show the average value of the nearest-neighbor interatomic distances for the Au_N clusters as a function of N. In this case, we have defined two atoms to be nearest neighbors if their interatomic distance is below the average of the nearest-neighbor and the next-nearest-neighbor distances of crystalline gold, i.e., below 6.58 a.u. The figure shows also experimental values for the Au_2 dimer and for crystalline gold as well as a typical theoretical value for a linear chain of gold atoms (see e.g., [25]). We see that our theoretical value for the Au_2 molecule is slightly larger than the experimental value. Moreover, we see that the average value even for the largest clusters of the present study, Au_{20}, is well below the value for the crystal but rather resembles the value for the linear gold chain, a system with low-coordinated gold atoms, as is the case for the present systems. In fact, as shown elsewhere [14], no atom for the gold clusters with up to 20 atoms have a higher coordination than 7, and for the largest clusters the average is around only 5.

As discussed previously [14], we found that the optimized structures of the Au_N clusters possess a low symmetry. Moreover, the clusters with up to $N = 6$ atoms were found be planar. Above $N = 6$, the structures are three-dimensional. On the other hand, experimental and theoretical studies suggest that planar structures are stable up to around 15 atoms (see e.g., [14, 20, 26, 27]). Therefore, we also considered these planar structures.

Figure 3 depicts the total energy variation as a function of cluster size. We see that the planar structures are energetically close to the global minimum isomers predicted by our unbiased genetic algorithm search. This suggests that the inaccuracies in the DFTB description of the interatomic interactions are small. On the other hand, the total energy of the icosahedral Au_{13} cluster is significantly above the value for the optimized Au_{13} cluster, whereas the tetragonal Au_{20} cluster is only marginally higher in energy than the globally optimized structure. In addition, when allowing the symmetry of the icosahedral Au_{13} cluster to be lowered, the total energy is reduced, too, as can be seen in the figure. This is to a much lesser extent the case for the tetrahedral Au_{20} cluster.

To identify particularly stable clusters, it is useful to consider the stability function,

$$\triangle_2 E(N) = E(N+1) + E(N-1) - 2E(N). \tag{10}$$

This function has maxima (minima) for particularly stable (unstable) clusters, see Fig. 4. Figure 4 shows a clear even-odd oscillatory pattern, implying that clusters with even N are more stable than those with odd N. Moreover, the cluster with $N = 8$ is found to be particularly stable. As we shall show below, this cluster may be ascribed an almost spherical shape, which can explain its enhanced stability. An additional reason may be found in its electronic properties: the cluster with $N = 8$ atoms has a particularly large energy gap between occupied and unoccupied orbitals (see [14]).

Information about the overall structure is obtained as follows. For each Au_N, cluster we first determine its center,

$$\mathbf{R}_0 = \frac{1}{N}\sum_{i=1}^{N} \mathbf{R}_i, \tag{11}$$

with $\mathbf{R}_i$ being the position atom i. Subsequently, we introduce a radial vector for each atom,

$$\mathbf{r}_i = \mathbf{R}_i - \mathbf{R}_0. \tag{12}$$

From the radial vectors, we construct the 3×3 matrix containing $\sum_i s_i\ t_i$ (with s and t being x, y, and z). The eigenvalues $I_{\alpha\alpha}$ of this matrix are used to identify the overall cluster-shape: three identical eigenvalues suggest a more spherical shape, whereas two large and one small value suggest a lens-like shape, and two small and one large value suggest a cigar-like shape. Figure 5 shows the average eigenvalue (divided by $N^{-\frac{5}{3}}$, which is the scaling a spherical jellium model has) together with marks indicating the overall shape. The figure also depicts the largest

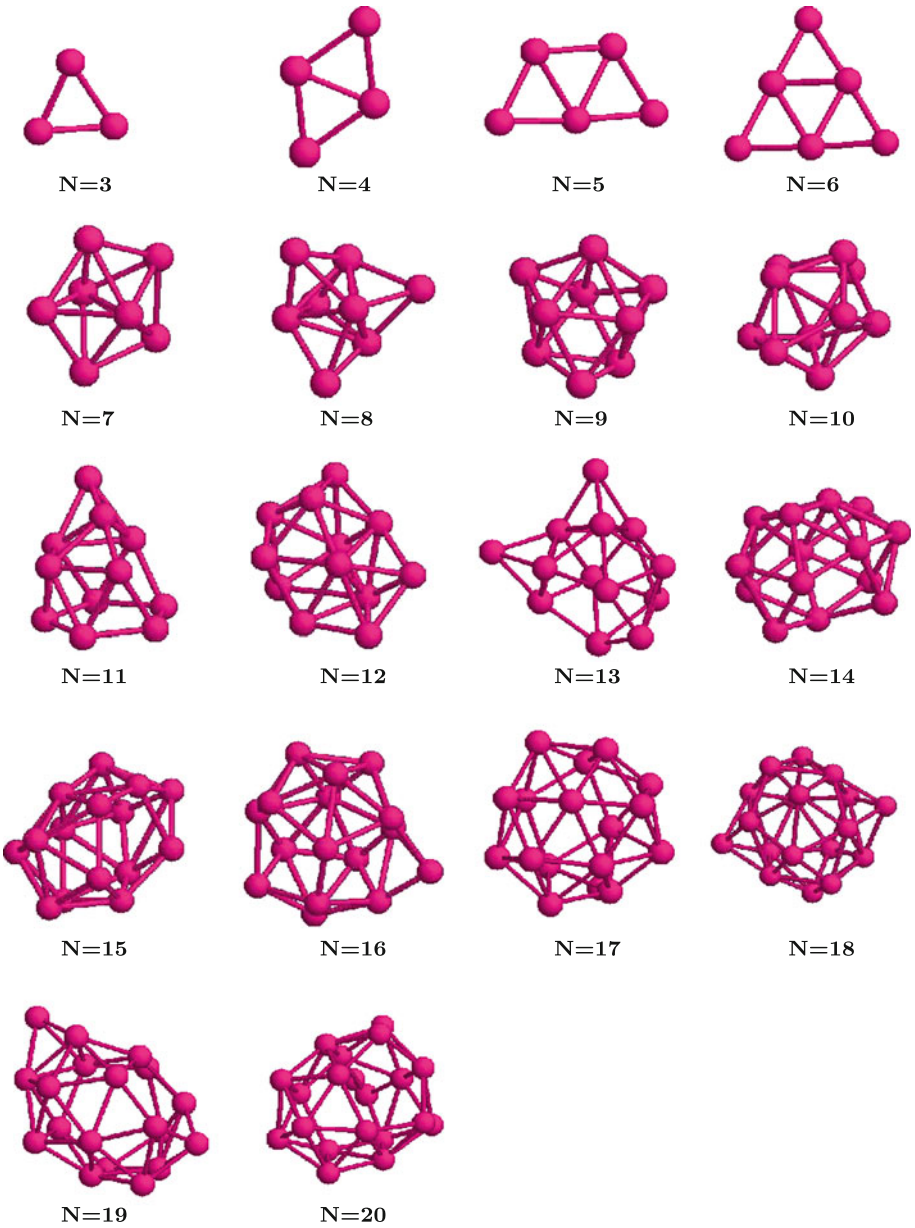

Fig. 1 The structures of the Au_N clusters from the global structure optimization

difference between the eigenvalues. We see that except for a single atom, no cluster has an overall spherical shape, which agrees with the point group analysis of our former study [14]. It is obvious that the clusters exhibit a low symmetry. However, for $N = 8$, 9, and 18, the largest difference of the eigenvalues is small (in particular for $N = 8$) suggesting that these clusters are close to being spherical. Fa et al. [28] suggested that the clusters could have structures related to either fragments of the crystal or tube-like structures. This is not supported by the results shown in Fig. 5; the structures are indeed of low symmetry.

We may use the common-neighbor analysis [29–31] to obtain further information on the cluster structures. First, a cut-off distance is defined to decide whether two atoms are assumed bound or unbound. Then, three indices (i, j, k) are ascribed to each pair of atoms. i is the number of common neighbors, j is the number of bonds between them, and k is the number of bonds in the longest unbroken sequence of bonds among them. We use the average of the nearest— and next-nearest-neighbor distances in the fcc crystal structure of Au as cut-off distance. For an infinite fcc crystal, the three sets (2,1,1), (4,2,1), and (4,4,4) occur with a relative occurrence of 4:2:1. Figure 6 exhibits many other sets of indices additional to those of the fcc crystal and with relative occurrences comparable with the ones of the indices of the fcc crystal. Thus, the common-neighbor analysis does not at all suggest that the structure of the clusters is similar to a crystal fragment.

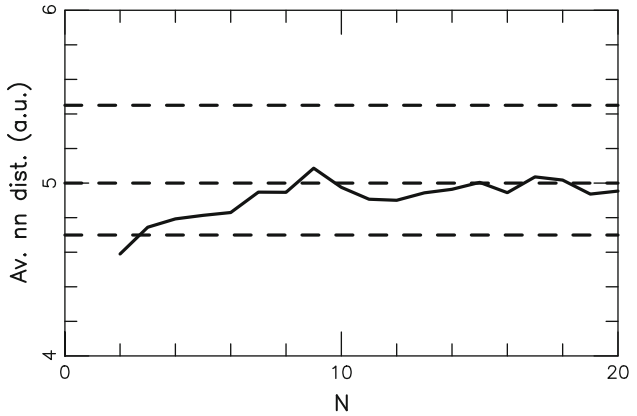

Fig. 2 The average nearest-neighbor bond length as a function of cluster size. The *horizontal dashed lines* give (from below) the experimental value for the gold dimer, the theoretical value for a linear chain of gold atoms, and the experimental value for crystalline gold

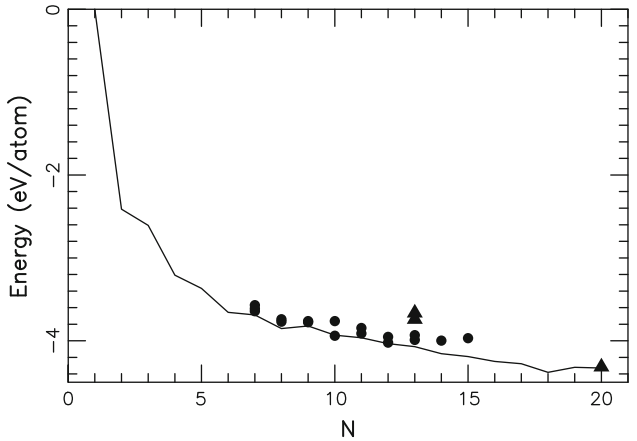

Fig. 3 The variation in the total energy per atom (relative to that of the isolated atom) for the optimized Au_N clusters (*solid curve*). In addition, for $N > 6$, our calculations give non-planar structures as the lowest-total energy structures. For $7 \leq N \leq 15$, we show, therefore, also the total energy of the planar structures (*dark circles*). For $N = 13$, we show also the total energy of icosahedral Au_{13} and for $N = 20$ also that of tetragonal Au_{20} clusters (*dark triangles*) both before (*upper symbols*) and after (*lower symbols*) structural relaxation

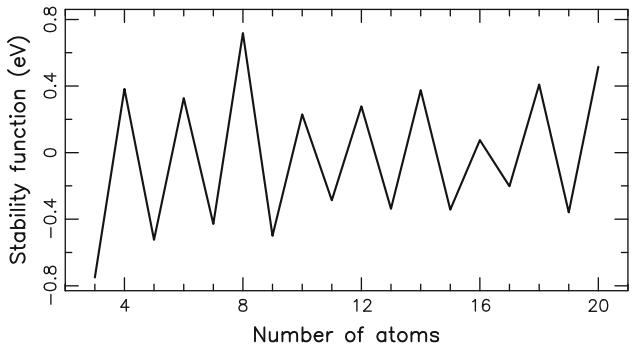

Fig. 4 The stability function as a function of N

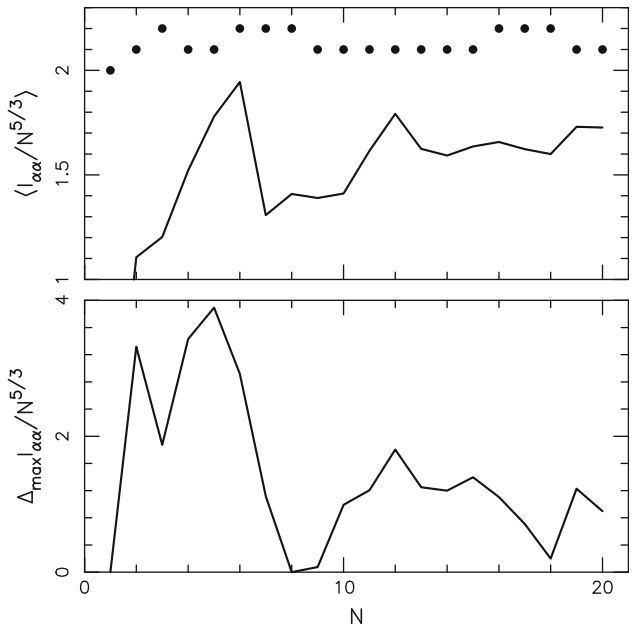

Fig. 5 Properties related to the eigenvalues $I_{\alpha\alpha}$ that describe the overall shape of the clusters. The *upper panel* shows the average value (scaled by $N^{-5/3}$) together with marks indicating whether the Au_N cluster is overall spherical (*dots* in the *lowest row*), overall cigar-like shaped (*middle row*) or overall lens-like shaped (*upper row*). The *lower panel* shows the largest difference in the eigenvalues

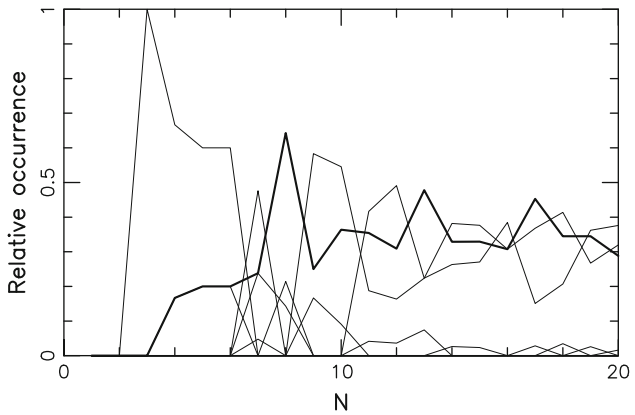

Fig. 6 Results of a common-neighbor analysis. Each *curve* shows the relative occurrence of a certain set of indices (i, j, k) (described in the text), when excluding $(i, j, k) = (0, 0, 0)$, and the thicker *curve* shows the occurrence for $(i, j, k) = (2, 1, 1)$. $(i, j, k) = (4, 1, 1)$ and $(i, j, k) = (4, 4, 4)$ are not found in this size range

3.2 Heat capacities and vibrational properties

As an extension of our earlier study, the optimized structures were used for calculating the vibrational contribution to the heat capacity at finite temperatures. Figure 7 shows the results for 70, 298.15, 500, 700, and 1,200 K. The vibrational heat capacity of the gold clusters shows a strong size dependence [beyond that of Eq. 9], particularly for smaller cluster sizes and at low temperatures. This feature

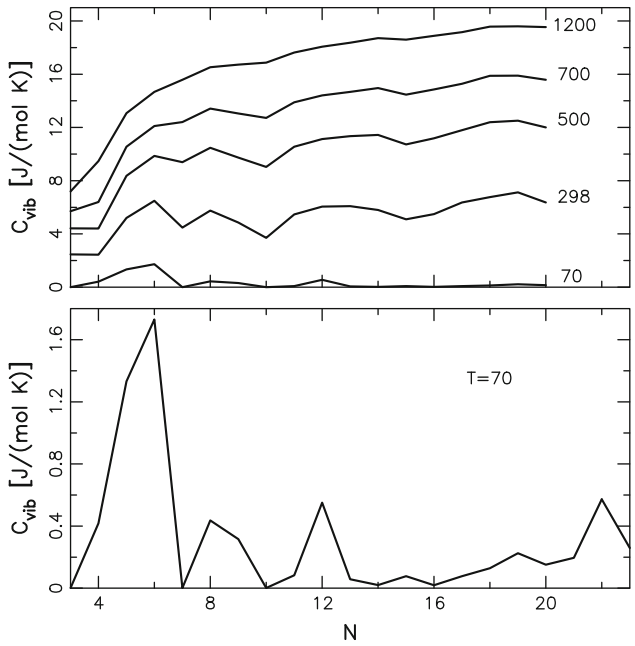

Fig. 7 The vibrational contribution to the heat capacity per cluster for different temperatures as function of size of the clusters. The *lower panel* shows an expanded version of the results for $T = 70$ K

becomes less pronounced as the cluster size and/or temperature increases. The obtained pattern does not compare to the stability function Fig. 4; the only coinciding peak is at $N = 6$ atoms. Thus, there seems to be little correlation between low-temperature vibrational heat capacity and stability.

Figure 8 shows C_{vib} as a function of temperature for different cluster sizes. As expected, for each size C_{vib} is a monotonously increasing function of T. Interesting is it that C_{vib} for $N = 6$ is a much more rapidly increasing function of T for low T than is the case for the other cluster sizes. Figure 7 reflects this finding as well.

It follows from Eq. 7 that C_{vib} is a superposition of the contributions from the individual modes. In Fig. 9, we show the contributions from the three modes with non-

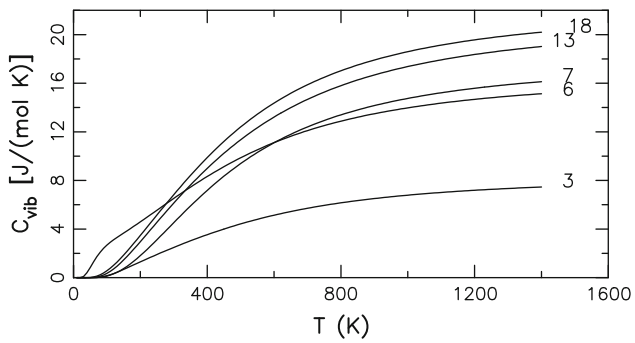

Fig. 8 Heat capacity as a function of temperature for clusters of different size

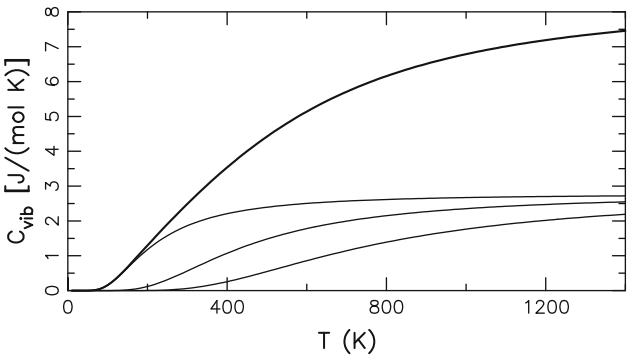

Fig. 9 The temperature dependence of the individual modes (*thin curves*) to the total vibrational heat capacity (*thick curve*) for the $N = 3$ cluster

vanishing frequencies for the cluster with $N = 3$ atoms. For a given temperature T, the contribution from the individual modes is a decreasing function of the frequency of the mode [see Eq. 7]. Thus, the largest contribution of the individual modes in Fig. 8 originates from the mode with the lowest frequency.

We can now rationalize the difference between the C_{vib} curves for $N = 6$ and the other cluster sizes (Fig. 8). Figure 10 presents the characteristic temperatures of the different modes as a function of cluster size. As discussed in Sect. 2, T_i quantifies the temperature range at which the contribution of the given mode changes most rapidly as a function of temperature. The atypical behavior of the $N = 6$ cluster in Fig. 8 is explained by the presence of a very low-frequency mode (i.e., a low T_i; see Fig. 10). Figure 10 suggests then that this will also be the case for the $N = 5$ and $N = 12$ clusters.

A similar analysis can also be used in order to explain the results for $T = 70$ K in Fig. 7. In this case, we have large values for C_{vib} in those cases where the smallest T_i is particularly small.

The reason that the $N = 6$ cluster has a mode with a particularly low characteristic frequency is found in the

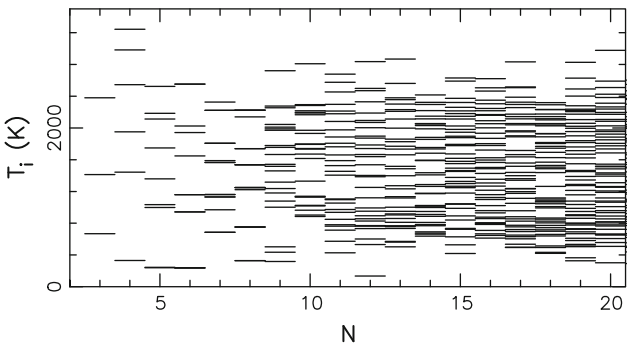

Fig. 10 The characteristic temperatures for the different vibrational modes as function of the size, N, of the clusters. For a given N, each *line* marks that at least one mode has that characteristic temperature

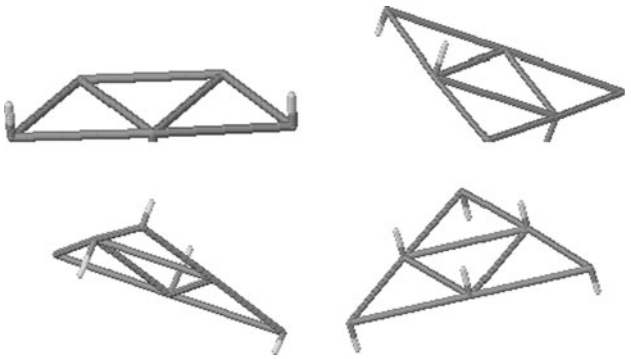

Fig. 11 Schematic representation of the vibrational modes of the lowest for Au_5 and Au_6. For the latter, three modes that are very close to being energetically degenerate are shown

calculated structural properties. According to our results, the gold clusters with up to $N = 6$ have a two-dimensional structure, whereas we find that from $N = 7$, the gold clusters form three-dimensional structures. The planar structure for $N = 6$ results in the energetically low-lying modes. Since it is known that also larger clusters are planar (as also found when using more accurate theoretical methods), it is possible that also the larger clusters will have particularly large heat capacities at low temperatures. In order to support this suggestion, we show in Fig. 11 a schematic representation of the modes of the lowest frequencies for the planar Au_5 and Au_6 clusters. For the latter, three modes are very close to being energetically degenerate and, therefore, we show all three modes. The figure clearly demonstrates that the low-energy modes for the planar clusters are related to a bending of the clusters.

4 Conclusions

We have presented the structural and thermodynamic properties of Au_N clusters with N from 2 to 20. We used an unbiased approach to identify the structures of the global total-energy minima. This method combines genetic algorithms with a parametrized density-functional method. As an extension of our earlier work, we have studied vibrational and thermodynamic properties of the clusters in order to explore relations between stability, structure, and heat capacities of clusters.

Our study shows that the gold clusters generally exhibit low symmetry, and that with up to $N = 6$, the clusters adopt planar structures. For larger values of N, our approach finds three-dimensional structures, which is in partly disagreement with more accurate methods. However, we find that the total-energy difference between planar and three-dimensional structures for N up to well above 10 is very small. By analyzing the structures, we find that the clusters do not resemble fragments of the fcc crystal. The vibrational heat capacity of the gold clusters is found to be strongly size dependent at low temperatures and for the smallest clusters. This becomes less pronounced when the size and/or temperature increases. An interesting observation is that the planar structures have a particularly large vibrational heat capacity at low temperatures, a finding that is related to the existence of low-frequency out-of-plane modes of these clusters and that might be used in experimentally identifying those.

Details about the total energies, the structures, and the lowest vibrational frequencies can be found in the supplementary material.

Acknowledgments This work was supported by the German Research Council (DFG) through project Sp439/23.

References

1. Rossi G, Ferrando R (2006) Chem Phys Lett 423:17
2. Donnelly RA (1994) Chem Phys Lett 136:274
3. Wales DJ, Doye JPK (1997) J Phys Chem 101:5111
4. Deaven DM, Ho KM (1995) Phys Rev Lett 75:288
5. Morris JR, Deaven DM, Ho KM (1996) Phys Rev B 53:R1740
6. Deaven DM, Tit N, Morris JR, Ho KM (1996) Chem Phys Lett 256:195
7. Ge Y-B, Head JD (2004) Chem Phys Lett 398:107
8. Ge Y-B, Heas JD (2004) J Phys Chem B 108:6025
9. Joswig J-O, Springborg M (2003) Phys Rev B 68:085408
10. Baletto F, Ferrando R (2005) Rev Mod Phys 77:371
11. Schmidt M, Donger J, Hippler T, Haberland H (2003) Phys Rev Lett 90:103401
12. Calvo F, Spiegelman F (2004) J Chem Phys 120:9684
13. Breaux GA, Neal CM, Cao B-P, Jarrold MF (2005) Phys Rev Lett 94:173401
14. Dong Y, Springborg M (2007) J Phys Chem C 111:12528
15. Seifert G, Porezag D, Fraunheim Th (1996) Int J Quantum Chem 58:185
16. Hohenberg P, Kohn W (1964) Phys Rev 136:B864
17. Kohn W, Sham LJ (1965) Phys Rev 140:A1133
18. Dong Y, Burkhart M, Veith M, Springborg M (2005) J Phys Chem B 109:22820
19. Goldberg DE (1986) Genetic algorithms in search optimization and machine learning. Addison-Wesley, Reading
20. Gilb S, Weis P, Furche F, Ahlrichs R, Kappes MM (2002) J Chem Phys 116:4094
21. Bonačić-Koutecký V, Burda J, Mitrić R, Ge M (2002) J Chem Phys 117:3120
22. Häkkinen H, Yoon B, Landman U, Li X, Zhai H-J, Wang L-S (2003) J Phys Chem A 107:6168
23. Li J, Li X, Zhai H-J, Wang L-S (2003) Science 299:864
24. Bowman JM (1986) Acc Chem Res 19:202
25. De Maria L, Springborg M (2000) Chem Phys Lett 323:293
26. Johansson MP, Lechtken A, Schooss D, Kappes MM, Furche F (2008) Phys Rev A 77:053202
27. Pyykkö P (2008) Chem Soc Rev 37:1967
28. Fa W, Luo C (2005) J Phys Rev B 72:205428
29. Hunnycutt JD, Andersen AC (1987) J Phys Chem 91:4950
30. Clarke AS, Jónsson H (1993) Phys Rev E 47:3975
31. Faken D, Jónsson H (1994) Comput Mater Sci 2:279